Guanine-Stabilized Formamidinium Lead Iodide Perovskites

Li Hong,[a,b] Jovana V. Milić,[a] Paramvir Ahlawat,[c] Marko Mladenović,[c] Dominik J. Kubicki,[a,d] Farzaneh Jahanabkhshi,[c] Dan Ren,[a] María C. Gélvez-Rueda,[e] Marco A. Ruiz-Preciado,[a] Amita Ummadisingu,[a] Yuhang Liu,[a] Chengbo Tian,[b] Linfeng Pan,[f] Shaik M. Zakeeruddin,[a] Anders Hagfeldt,[f] Ferdinand C. Grozema,[e] Ursula Rothlisberger,[c] Lyndon Emsley,[d] Hongwei Han*[b] and Michael Graetzel*[a]

Abstract: Formamidinium (FA) lead iodide perovskite materials feature promising photovoltaic performances in conjunction with superior thermal stabilities. However, the conversion of the perovskite α-$FAPbI_3$ phase to the thermodynamically stable yet photovoltaically inactive δ-$FAPbI_3$ phase compromises the photovoltaic performances of the corresponding solar cells. Herein, we demonstrate a novel strategy for overcoming this challenge by employing low-dimensional hybrid perovskite materials comprising guaninium (G) organic spacer layers that act as stabilizers of the three-dimensional α-$FAPbI_3$ phase. Furthermore, we unravel the underlying mode of interaction at the atomic level by means of solid-state nuclear magnetic resonance spectroscopy in conjunction with X-ray crystallography, transmission electron microscopy, molecular dynamics simulations and DFT calculations. As a result, we obtain low-dimensional-phase-containing hybrid $FAPbI_3$ perovskite solar cells with improved performances, accompanied by enhanced long-term stability.

Introduction

Hybrid perovskite solar cells (PSCs) present a new generation of thin-film photovoltaic technologies featuring hybrid organic-inorganic perovskite semiconductors.[1-4] They are based on AMX_3 stoichiometry composed of a monovalent cation A (Cs^+, methylammonium (MA) $CH_3NH_3^+$, formamidinium (FA) $CH(NH_2)_2^+$, or guanidinium (GUA) $C(NH_2)_3^+$), a metal M (Pb^{2+}, Sn^{2+}), and a halide X (Cl^-, Br^-, or I^-). While hybrid perovskites display remarkable solar-to-electric power conversion efficiencies (PCE), practical applications are still hampered by their instability towards ambient air and moisture as well as thermal and light stress.[2,3] PSCs featuring highly polar MA organic cations (dipole moment of 2.29 D) are more sensitive to moisture and polar solvents, posing the risk of long term instability.[5] Alternatively, hybrid perovskite materials based on FA organic cation (dipole moment of 0.21 D) are characterized by a more homogenous distribution of the electron density due to resonance stabilization that reduces their reactivity, rendering the corresponding material more stable, in particular against thermal stress.[5,6] Moreover, the larger FA cation size increases the lattice constant and the degree of space filling, [7,8] and its perovskite structure is further stabilized by stronger hydrogen bonding as compared to the MA analogs.[8] However, $FAPbI_3$ exists in two phases, namely the yellow δ-$FAPbI_3$, which is more thermodynamically stable at room temperature, and the black α-$FAPbI_3$ perovskite phase that is of interest to photovoltaic applications.[9,10] Stabilizing the black α-$FAPbI_3$ perovskite phase without significantly altering its optoelectronic properties remains an ongoing challenge that could boost further optoelectronic applications. This has been predominantly achieved by using Cs^+ cations,[11,12] which however increase their bandgap. It has been recently shown that a number of FA-based layered low-dimensional perovskites can stabilize $FAPbI_3$ perovskite solar cells via their spacer layer.[13-15] However, these early examples mainly employ electronically insulating organic spacers, such as the prototypical butylammonium (BA) and phenylethylammonium (PEA),[13,14] as well as more elaborate analogs, such as the 1-adamantanemethylammonium (ADA) and 1,4-phenylenedimethylammonium (PDMA),[15-16] with photovoltaic performances that are inferior to the 3D perovskites. Alternatively, a number of 2D/3D heterostructures has been developed employing the 2D structures as stabilizing layers,[11,12] yet this effort has been mainly focused on mixed A-cation compositions. Moreover, the contribution of the low dimensional layer to the overall performance is limited, particularly as a result of the insulating character of the organic spacer layers.[17] It is therefore instrumental to set the stage for the development of functionalized layered hybrid perovskites comprising electroactive organic spacers that can play a stabilizing role in hybrid perovskite heterostructures while raising the device performance.

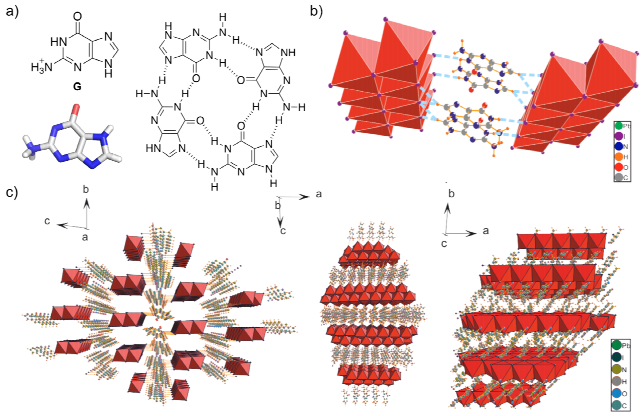

Figure 1. (a) Structure of guaninium (G) with its DFT-optimized (B3LYP/6-31G(d)) geometry (left) and common supramolecular assemblies, such as the G-quadruplex (right). (b) Schematic highlighting the interactions between G and PbI_2 in the G_2PbI_4 crystal structure. (c) Crystal structure of G_2PbI_4 along a, b, c-axis, respectively. Solvent molecules are omitted for clarity.

[a] Li Hong, Dr. Jovana V. Milić, Dr. Dominik J. Kubicki, Dr. Dan Ren, Dr. Marco Alejandro Ruiz-Preciado, Dr. Amita Ummadisingu, Dr. Yuhang Liu, Dr. Shaik M. Zakeeruddin, and Prof. Michael Graetzel*
Laboratory of Photonics and Interfaces, Institut des Sciences et Ingénierie Chimiques, École Polytechnique Fédérale de Lausanne, 1015 Lausanne, Switzerland
E-mail: michael.graetzel@epfl.ch
[b] Li Hong, Chengbo Tin, and Prof. Hongwei Han*
Wuhan National Lab for Optoelectronics
Wuhan, 430074 Hubei, China
E-mail: hongwei.han@mail.hust.edu.cn
[c] Paramvir Ahlawat, Dr. Marko Mladenović, Farzaneh Jahanbakhshi, and Prof. Ursula Rothlisberger
Laboratory of Computational Chemistry and Biochemistry, Institut des Sciences et Ingénierie Chimiques, École Polytechnique Fédérale de Lausanne, 1015 Lausanne, Switzerland
[d] Dr. Dominik J. Kubicki and Prof. Lyndon Emsley
Laboratory of Magnetic Resonance, Institut des Sciences et Ingénierie Chimiques, École Polytechnique Fédérale de Lausanne, CH-1015 Lausanne, Switzerland
[e] María C. Gélvez-Rueda and Prof. Ferdinand C. Grozema
Delft University of Technology, 2629 HZ Delft, The Netherlands
[f] Linfeng Pan and Prof. Anders Hagfeldt
Laboratory of Photomolecular Science, Institut des Sciences et Ingénierie Chimiques, École Polytechnique Fédérale de Lausanne, 1015 Lausanne, Switzerland

Supporting information for this article is given via a link at the end of the document.

Herein, we demonstrate the utility of guaninium (G)-derived low-dimensional perovskites in stabilizing the α-$FAPbI_3$ perovskite phase, which is assessed by solid-state NMR spectroscopy, X-ray crystallography, molecular dynamics simulations, and DFT calculations. Guanine is a biologically relevant organic molecule that plays an important role in stabilizing the DNA structure (Figure 1a), while displaying the propensity for the formation of conductive supramolecular assemblies and functional materials.[18-21] We have therefore utilized its functional units to form a novel hybrid perovskite structure based on the low dimensional G_2PbI_4 composition, which was used to increase the performance and stability of α-$FAPbI_3$ perovskite solar cells.

Results and Discussion

We synthesized G_2PbI_4 by mixing guaninium iodide (GI; Figure 1a and Figure S1 in the Supporting Information, SI) and lead iodide (PbI_2) in 2:1 molar ratio in γ-butyrolactone (GBL) as a solvent and heating the solution to 70 °C until dissolved. The experimental details are provided in Section S1 of the SI. Hydroiodic acid was added into the turbid solution to fully dissolve the solute at concentration of 0.1 M. The crystal structure of the resulting solvated G_2PbI_4 intermediate reveals intermolecular hydrogen bonding (HB) between the organic spacer layer and inorganic sheets (Figure 1b–c). Formation of HB adducts was consistent with the Fourier transform infrared (FT-IR) spectra of the thin films of GI, GI•PbI_2 and GI•PbI_2•FAI (shown in Figure S2a in the Supporting Information, SI) indicating that –N-H and $–NH_3^+$ stretching vibrations shift to higher frequencies for GI•PbI_2 and GI•PbI_2•FAI. Moreover, the differential scanning calorimetry (DSC) and thermal gravimetric analysis (TGA) of GI•PbI_2, PbI_2 and GI (Figure S2b in the SI), show different properties for the three species. During annealing up to 400 °C, there is no weight loss for PbI_2 while GI displays only one exothermic peak at around 290 °C. In the case of GI•PbI_2 two distinct exothermic peaks are observed at around 257 °C and 327 °C, corresponding to the weight loss in the range of 250–300 °C and 300–350 °C, respectively, further suggesting the presence of interactions between GI and PbI_2 in the G_2PbI_4 system.

To characterize these interactions at the atomic level, we have prepared non-solvated G_2PbI_4 by mechanosynthesis[22-23] and used ^1H, ^{13}C and ^{15}N solid-state magic angle spinning (MAS) NMR at 21.1 T to characterize it (for more details see Section S2 in the Supporting Information, SI). It has been shown that structural properties of hybrid perovskites[24-27] as well as their modulated[28,29] and layered low-dimensional analogues[15] can be assessed at the atomic level by means of solid-state NMR spectroscopy and that mechanochemically prepared samples correspond well to those fabricated by solution deposition. The ^{13}C CP MAS spectrum of unprotonated guanine shows five well-resolved resonances, corresponding to the inequivalent sites of the purine ring system (Figure 2a). Protonation of guanine with HI, yielding GI, leads to changes in the chemical shift of all peaks, as well as to the appearance of new peaks, likely due to the protonation of both the primary ($pK_a = 12.3$) and secondary ($pK_a = 9.2$) amine group of guanine (Figure 2b).[30,31] The formation of G_2PbI_4 is evidenced by changes in the ^{13}C NMR spectrum as compared to neat GI (Figure 2c), although peak assignment is difficult due to the high level of disorder. Analogous qualitative changes are visible in ^{15}N (Figure S3a–b, SI) and ^1H (Figure S3d–f, SI) solid-state NMR spectra. This spectral complexity may be partly associated with guanine adopting several tautomeric forms (Figure 2g).[30] Previous reports suggest that G exists in the aqueous phase as a mixture of two tautomers (Figure 2g), the *N*9H (85%) and a *N*7H form (15%). Moreover, *N*7H has been shown to be more stable than *N*9H form in solution, although the latter was found to be the only tautomer in polar solvents or in the solid state.[30] Protonation was reported to predominantly occur at position *N7*, which is also suggested by the corresponding p*K*a values.[31] As a result, hydrogen bonding of protonated G units leads to the formation of regioisomeric dimers (Figure 2h), which further contributes to the broadening of the NMR spectra of GI, G_2PbI_4 and hybrid $FAPbI_3$ composites with GI (Figure 2d–f).

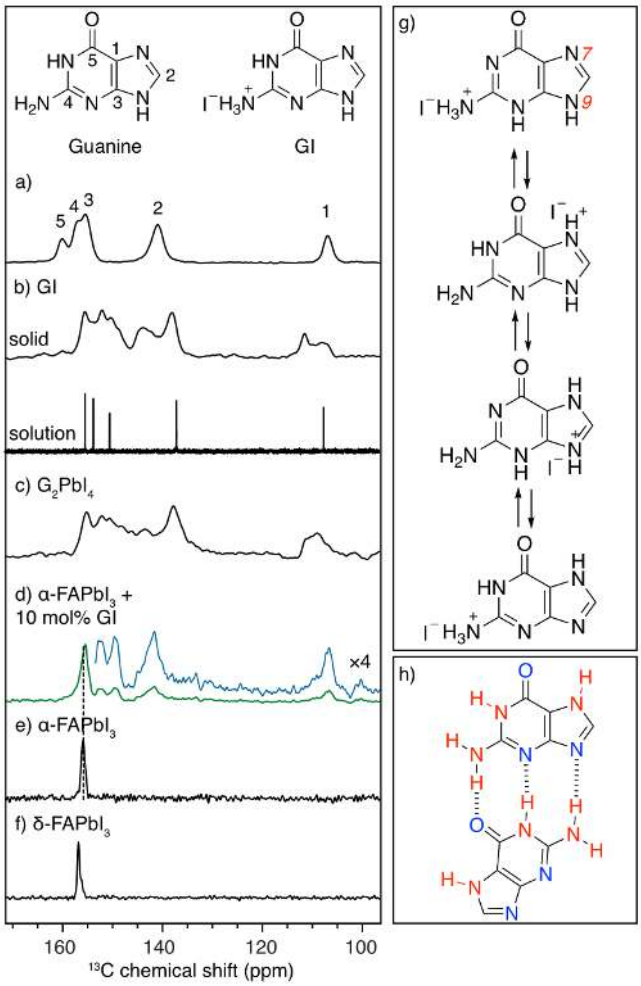

Figure 2. ^{13}C CP MAS spectra at 21.1 T, 298 K and 20 kHz MAS of (a) guanine, (b) guanine hydroiodide (G · HI or GI) in solid-state (upper) and solution of DMSO-d_6 (lower), and bulk mechanochemical (c) G_2PbI_4, (d) α-$FAPbI_3$ with 10 mol% GI, (e) α-$FAPbI_3$, and (f) δ-$FAPbI_3$. ^{15}N solid-state MAS NMR spectra at 21.1 T, 100 K, 12.5 kHz are shown in Figure S3 in the SI. (g) Structures of some of the tautomeric forms of GI (atomic numbering is highlighted in red, with alternative protonation sites being *N7* and *N*9) in equilibrium. (h) A representative hydrogen-bonded (HB) dimer of two guanine molecules with hydrogen-bond donating (red) and hydrogen-bond accepting (blue) sites.

For further structural insight, we analyzed the X-ray diffraction (XRD) patterns of G_2PbI_4 films on FTO/compact (c-)TiO_2/mesoporous (mp-)TiO_2 substrates (Figure 3a). The thin films were prepared by the hot-casting method (more details are provided in the Section S1 of the SI).[32] XRD patterns show two characteristic diffraction peaks at 2θ of 6.0 ° and 7.1 °, which are located in the low angle region, typical for low-dimensional perovskites. The broadening of the XRD signals is consistent with the presence of disorder visible in solid-state NMR spectra. Another unique signature of low-dimensional iodoplumbate phases is the presence of excitonic features in their UV-Vis absorption spectra.[33] We have therefore measured the UV-vis spectra of the corresponding films (Figure 3b), which show two absorption band edges at around 425 nm and 525 nm, likely corresponding to the excitonic peaks of the low-dimensional phases. These spectral features are consistent with the results of steady-state photoluminescence (PL; Figure 3b, inset) with Stokes shifts of approximately 25 nm, which is further in accordance with the formation of low-dimensional G_2PbI_4 phase.

Having identified the formation of G_2PbI_4, we probed its effect on the stability of α-$FAPbI_3$. The corresponding films and devices were fabricated via a one-step deposition method by spin-coating the precursor solutions without employing an anti-solvent (as detailed in the Section S1 of the SI). The mixed G/FA perovskite precursor solutions were prepared based on the $G_2FA_{n-1}Pb_nI_{3n+1}$ formula (with *n* corresponding to 1, 10, 20, 30, while n = ∞ indicates neat $FAPbI_3$), which defines the stoichiometry of the precursors without making any assumptions regarding the resulting crystal structure. The changes in color of the thin films deposited on FTO/c-TiO_2/mp-TiO_2 substrates were indicative of G-induced 3D perovskite stabilization, as films based on G-containing compositions appeared darker and maintained their color for a longer period in ambient conditions (Figure 3c), whereas neat $FAPbI_3$ films turned yellow during the same period of time. This suggests that the presence of G may stabilize the black α-$FAPbI_3$ phase. To corroborate this effect, we analyzed the XRD patterns of the neat $FAPbI_3$ and perovskite films based on the mixed $G_2FA_{n-1}Pb_nPbI_{3n+1}$ (n = 10, 20 and 30) compositions on FTO/c-TiO_2/mp-TiO_2 substrates. The XRD patterns immediately after the preparation (Figure 3d) reveal the presence of the hexagonal δ-$FAPbI_3$ phase diffraction peak at 11.8° for neat $FAPbI_3$ perovskite films, while this peak is not present in the G-containing compositions. After 5 weeks of storage in the dark at 20–25 °C in ambient air of relative humidity (RH) of ~40%, the peak intensity of δ-$FAPbI_3$ sharply increased compared to that of α-$FAPbI_3$ for the neat perovskite films (Figure 3e). On the contrary, the phase transformation was suppressed in the G-containing perovskite films, especially in the films based on the n = 20 composition. However, a strong diffraction peak of δ-$FAPbI_3$ was observed in the n = 10 composition, which is likely to be the result of poor film morphology owing to the low solubility of GI in organic solvents. In this regard, presence of secondary non-perovskite phases may be detrimental to long-term stability under ambient conditions, facilitating perovskite degradation processes.[34] In addition, a low angle diffraction peak at 6.0 ° was observed for both fresh and aged perovskite films of n = 10 composition, indicating the presence of a low-dimensional iodoplumbate structure. In the case of n = 20, this peak was not present in the XRD pattern, presumably as a result of the lower concentration of the low-dimensional phase. We have assessed the structural changes by X-ray photoelectron spectroscopy (XPS) of neat and n = 20 perovskite films (Figure S4, SI). The XPS spectra show a peak centered at 399.0 eV in the N 1s spectral domain for the n = 20 perovskite films, which can be ascribed to the C=N bond of G. In addition, the Pb core level 4*f* 7/2 and 4*f* 5/2 peaks of n = 20 systems shift to lower binding energies as compared to neat $FAPbI_3$, indicating changes in the structure, likely as a result of the interaction with G. This interaction-induced structural change that appears to be more stabilizing at lower concentrations of guanine suggests a structure-directing role,[28,29] which was also assessed at the atomic level by solid-state NMR spectroscopy.

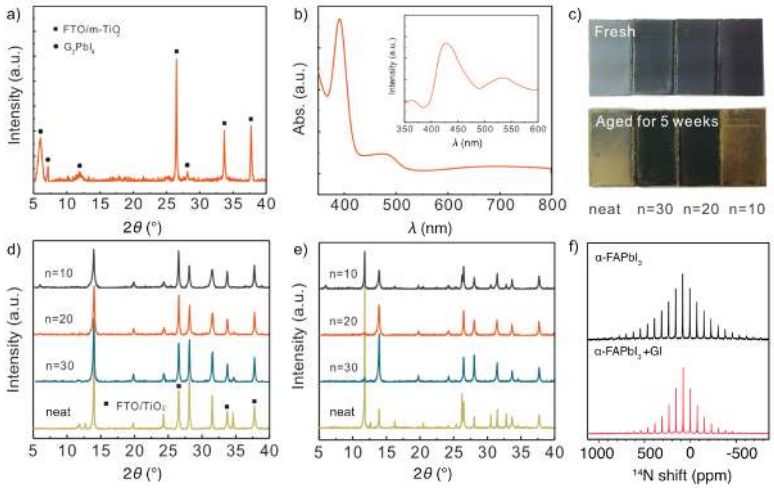

Figure 3. (a) X-ray diffraction (XRD) patterns and (b) UV-vis spectrum of G_2PbI_4 films, with the corresponding steady photoluminescence (PL) spectrum shown in the inset. (c) Pictures of the corresponding perovskite films. (d-e) XRD patterns for neat $FAPbI_3$ and mixed perovskite films of $G_2FA_{n-1}Pb_nPbI_{3n+1}$ composition (formal stoichiometries of n = 10, 20 and 30) on FTO/c-TiO_2/m-TiO_2 substrates (d) immediately after preparation and (e) upon aging for 5 weeks, respectively. Enlarged XRD patterns are shown in the Figure S2 of the Supporting Information. (f) ^{14}N solid-state magic angle spinning NMR spectra at 21.1 T, 298 K, 5 kHz of bulk mechanochemical α-$FAPbI_3$ (top) and G-containing α-$FAPbI_3$ (10 mol% GI; bottom) powders.

We analyzed the microstructure of bulk mechanochemical $FAPbI_3$ doped with 10 mol% GI by solid-state NMR spectroscopy (Figure 2d–f and Figure S3, SI). ^{13}C MAS NMR spectrum of this formulation contains four well-resolved G peaks (Figure 2d–f) corresponding to carbons 1 (107 ppm), 2 (142 ppm), 3 (150 ppm), 4 (153 ppm), which are markedly different from those of neat GI or G_2PbI_4 and therefore evidence the formation of a new G/FA-based iodoplumbate phase (Figure 2b–d). The peak of carbon 5 overlaps with the FA signal of α-$FAPbI_3$ (155 ppm). This change in the underlying atomic-level microstructure allows to rationalize the change in the binding energies of the Pb core levels observed by XPS. Moreover, we have previously shown that ^{14}N NMR can be used as a sensitive diagnostic tool for structural changes of $FAPbI_3$.[15,28,29] Specifically, the width of the spinning side band (SBB) pattern of ^{14}N NMR signals are determined by the local cubooctahedral symmetry of FA, which is tumbling in the ps regime. Consequently, narrower ^{14}N SSB manifolds indicate higher cubooctahedral symmetry (closer to cubic). α-$FAPbI_3$ containing with 10 mol% GI has a narrower ^{14}N SSB manifold than neat α-$FAPbI_3$, which shows that the crystallographic symmetry of the 3D perovskite is affected by the presence of GI such that it increases the cubooctahedral symmetry (Figure 3f). We suggest that this may contribute to the improved electronic quality of the thin films. To gain further understanding of this perovskite structure, we analyzed the perovskite films of $G_2FA_{n-1}Pb_nPbI_{3n+1}$ (n = 20) by transmission electron microscopy (TEM; Figure 4). The representative TEM image of the polycrystalline film shows a grain and its boundary (Figure 4a). A high-resolution (HR) image of the area (indicated by a square in Figure 4a) and its Fast Fourier Transform (FFT) reveals an inter-planar spacing of 0.32 nm (Figure 4c), which matches the (002) reflection of the cubic α-$FAPbI_3$ perovskite phase. In addition, an interplanar distance of 0.74 nm is revealed, which corresponds well to the size of the G spacer (7.5 Å) inside the G_2PbI_4 phase (Figure 1b). This suggests that the low-dimensional G_2PbI_4 phase exists along the grain boundaries of the α-$FAPbI_3$, which can account for its stabilization in the hybrid G-containing α-$FAPbI_3$ compositions. This result is in line with the NMR analysis, which shows the formation of new G environments modified by the proximity of the 3D perovskite phase in the hybrid G-containing α-$FAPbI_3$ system.

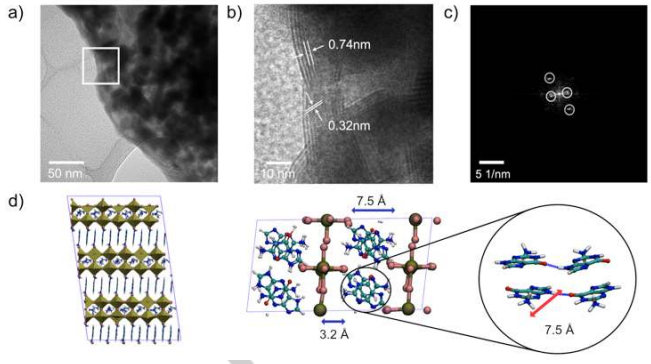

Figure 4. TEM images of $G_2FA_{n-1}Pb_nPbI_{3n+1}$ (n = 20) perovskite compositions: (a) A lower magnification image and (b) high resolution image of the marked area in a) with (c) the corresponding Fourier transform (FFT) analysis. (d) DFT-optimized structure of $G_2FAPb_2I_7$. For more details refer to the Section S3 in the Supporting Information.

A mechanistic model that could explain the formation of such mixed hybrid perovskite structures must consider a number of different tautomeric forms as well as their propensity to dimerization via hydrogen bonding without interfering with the formation of a low-dimensional phase (Figure 2g–h). Furthermore, the resulting structures should take into consideration the properties of the solvated G_2PbI_4 intermediate revealed by single crystal XRD (Figure 1c). We assessed the possible structural models by molecular dynamics (MD) simulations based on both classical and DFT calculations starting from the intermediary G_2PbI_4 solvated crystal structure (for more details refer to Section S3 in the SI). We analyzed a number of possible low-dimensional structures based on G_2PbI_4 and $G_2FAPb_2I_7$ compositions as model systems (Figures S7–S18, SI), and compared them to the experimental findings. As a result of this analysis, we identified a unique and stable structure composed of alternating hydrogen-bonded G dimers inside the spacer layer, oriented such that both HB of the spacers and their interaction with the perovskite slabs is possible (Figure 4d and Figures S11–S12, SI). The structural properties of the resulting system matched well the spacer dimensions revealed by both the TEM (Figure 4d) and XRD measurements (Figure S14, SI). Moreover, DFT calculations of the structures suggest that proton transfer occurs between the molecules in the spacer layer, which supports the existence of multiple tautomeric forms (for more details, refer to the Section S3 in the SI). This suggests that the formation of G-based low-dimensional structures involves a reorientation of the spacer molecules to form HB within the spacer (Figure S13, SI), while simultaneously binding to the inorganic slabs. In this fashion, the G-based spacer layer could affect proton transfer in addition to providing enhanced transport for electronic charge carriers. A more detailed mechanistic insight requires extensive nucleation studies that are subject of an ongoing investigation.

To evaluate this model, we analyzed the optoelectronic properties of neat $FAPbI_3$ and mixed $G_2FA_{n-1}Pb_nPbI_{3n+1}$ (n = 10, 20 and 30) perovskite films on FTO/c-TiO_2/mp-TiO_2 substrates (Figure 5). The UV-Vis absorption spectra suggest that the absorbance of the films of both n = 20 and 30 is much higher than that of neat α-$FAPbI_3$ films, presumably due to improved phase purity and film uniformity (Figure 5a). The films of n = 10 show absorbance that is lower than that of n = 20 and 30 perovskites, whereas top-view scanning electron microscopy (SEM; Figure S5, SI) images indicate that the grain sizes do not evidently change with the increasing *n* value. The effect of G_2PbI_4 perovskite on the optical band gap was probed by analyzing the corresponding Tauc plots (Figure 5b-c). For $G_2FA_{n-1}Pb_nPbI_{3n+1}$ (n = 10, 20, 30) compositions, the band gap remained around 1.51 eV, exceeding the value of α-$FAPbI_3$ by only 30 meV.[35,36] We can thus conclude that the presence of G does not affect the band gap of α-$FAPbI_3$ significantly, enabling the G-based perovskite composites to retain the advantages of the low band gap. However, the steady-state PL spectra (Figure 5d) reveal a minor blue-shift with certain asymmetry of the spectrum for n = 10, indicating that a higher ratio of low-dimensional phases may affect the optoelectronic properties. The time-resolved photoluminescence (TRPL) spectra of neat α-$FAPbI_3$ and mixed $G_2FA_{n-1}Pb_nPbI_{3n+1}$ (n = 10, 20, 30) films on glass microscope slides show a slightly longer charge carrier lifetimes for n = 20 as compared to the other compositions, pointing at suppressed charge carrier recombination (Figure 3e).

We further measured the TRPL spectra of perovskite/spiro-OMeTAD structure on a glass slide to assess the effect on charge carrier transport at the interface between the perovskite and spiro-OMeTAD. The mixed $G_2FA_{n-1}Pb_nPbI_{3n+1}$ perovskite materials were found to quench the PL of the 3D perovskite phase faster, with the n = 20 system showing the most pronounced effect, indicating the most enhanced charge transfer at the interface, a metrics which is important for the photovoltaic (PV) performance.

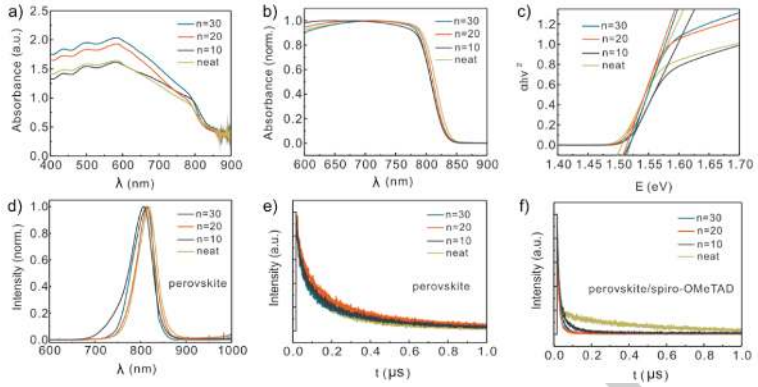

Figure 5. Optoelectronic properties of neat $FAPbI_3$ and mixed perovskite films of $G_2FA_{n-1}Pb_nPbI_{3n+1}$ (n = 10, 20 and 30) compositions. (a) UV-Vis absorption spectra, (b) normalized absorption spectra and the (c) corresponding Tauc plots on FTO/c-TiO_2/m-TiO_2 substrates; (d) steady-state and (e-f) time-resolved PL (TRPL) spectra for films on a microscope glass slide. The steady-state PL spectra of G_2PbI_4 is shown in Figure 3b.

This finding corroborates with the calculated electronic properties of the layered G_2PbI_4 structure (for details see Section S3.5 in the SI and Figures S19–S20), which suggest that the conduction band of the low-dimensional structure is delocalized within the spacer layer. This has been previously observed for a very few cases of low-dimensional perovskite structures[37,38] based on functional organic spacers that can serve as a pathway for charge transport, facilitating charge extraction. Moreover, the calculated hole effective masses along the three principal axes reveal reduced hole effective masses for in-plane directions coinciding with the π-stacking of the guanine moieties, suggesting a pathway for efficient hole transport. In order to clarify this, the mobility of charge carriers and photoconductivity (product of mobility and yield of charge dissociation) were determined by time-resolved microwave conductivity measurements (Section S4, SI and Figures S21–S23).[39,40] The measurements revealed conductivities that increase for n = 20 as compared to the n = 1 compositions, which is accompanied by charge carrier lifetimes in the order of μs that is of interest to the PV applications. The photovoltaic metrics of neat α-$FAPbI_3$ and hybrid $G_2FA_{n-1}Pb_nPbI_{3n+1}$ (n = 10, 20 and 30) PSCs with an aperture area of 0.16 cm^2 (Figure 6) show that the n = 20 PSCs outperform those of neat α-$FAPbI_3$. The improvement can be ascribed to the stabilization of the α-$FAPbI_3$ in presence of the G-based phase. With the highly increased content of the low-dimensional component, as in the n = 10 compositions, however, the PV performance decreases. This is in accordance with the effect on the optoelectronic properties (Figure 5a and Section S4, SI). The comparatively poorer performance of the n = 30 compositions presumably results from the decrease in the film uniformity and optical properties as compared to the neat $FAPbI_3$ perovskite. This suggests that the optimal concentration thereby lies in the range between the ones defined by the n = 10 and n = 30 nominal compositions. As a result, we achieved PCEs up to 16.04% for hybrid $G_2FA_{n-1}Pb_nPbI_{3n+1}$ PSCs based on n = 20 compositions with V_{OC} of 1.08 V, J_{SC} of 22.08 mA cm^{-2}, and FF of 0.67. These parameters are superior to those of neat α-$FAPbI_3$, yielding a PCE of 8.42% with a V_{OC} of 0.74 V, J_{SC} of 18.59 mA cm^{-2}, and FF of 0.61 based on the reverse scan (Figure 6a). The hysteresis effects however remain apparent in the PSCs (Figure S6, SI). The corresponding incident photon-to-current conversion efficiency (IPCE) spectra show that the integrated J_{SC} of n = 20 PSC is 21.75 mA cm^{-2}, comparable to the value derived from the *J-V* curve, while the integrated J_{SC} of neat $FAPbI_3$ PSC is 13.87 mA cm^{-2}, lower than the one derived from the *J-V* curve. This is ascribed to the instability of untreated α-$FAPbI_3$, leading to its degradation during the measurement (the maximum power point tracking is shown in Figure S6 of the Supporting Information), which has been affected by the presence of guanine moieties.

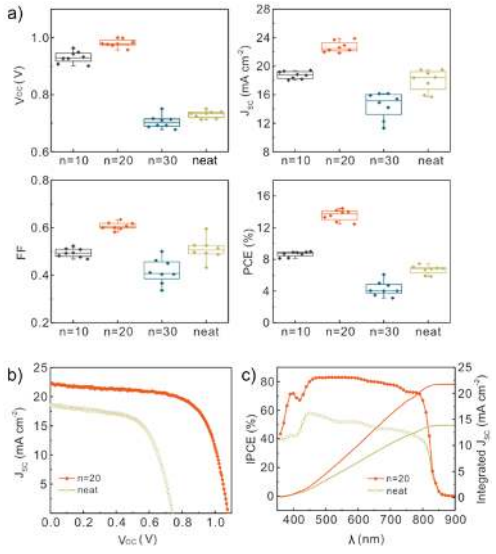

Figure 6. (a) PV metrics of 32 solar cells based on neat $FAPbI_3$ and mixed low-dimensional $G_2FA_{n-1}Pb_nPbI_{3n+1}$ (n = 10, 20 and 30) perovskite compositions; (b) *J-V* curves and (c) corresponding IPCE spectra with integrated J_{SC} of the best performed solar cells based on neat $FAPbI_3$ and perovskites of $G_2FA_{n-1}Pb_nPbI_{3n+1}$ (n = 20) composition. The aperture area of the devices is 0.16 cm^{-2}.

Conclusion

In summary, we developed a new strategy based on guaninium (G) moieties to tune the properties of α-$FAPbI_3$. We used solid-state NMR to establish that G interacts with the perovskite lattice at the atomic level, leading to the formation of mixed G/$FAPbI_3$ phases. We report the crystal structure of a low-dimensional G-based phase, which evidences the possible binding modes involved in the stabilization of α-$FAPbI_3$. Furthermore, we provide a mechanistic model for the formation of the G-based perovskite phase using molecular dynamics simulations and DFT calculations, which show that the guanine moieties have the propensity to enhance the transport of protons as well as charge transport through delocalization of the conduction band across the spacer layer. These findings were used to design solar cells based on hybrid $G_2FA_{1-n}Pb_nI_{3n+1}$ composition and obtain PCEs of over 16%, highlighting the prospect of this approach in metal halide perovskite photovoltaics.

Experimental Section

Synthesis and characterization of the materials, as well as the corresponding devices, are detailed in the Supporting information.

Acknowledgements

J.V.M, S.M.Z., and M.G. are grateful to the European Union's Horizon 2020 research and innovation program under grant agreement No. 826013 (IMPRESSIVE) as well as the GRAPHENE Flagship Core 2 project supported by the European Commission H2020 Programme under contract 785219. D.J.K. and L.E. acknowledge support from Swiss National Science Foundation Grant No. 200020_178860. D.R. acknowledges the SNSF grants IZLCZ2-170294 and IZJSZ2_180176. U.R. acknowledges SNSF Grant No. 200020-165863, NCCR-MUST, NRP70, and the SINERGIA interdisciplinary research program EPISODE for funding. Y.H, Y.R, and H.H. acknowledge financial support from the National Natural Science Foundation of China (Grant Nos. 21702069, 51502141, 91733301, 91433203 and 61474049), the Ministry of Science and Technology of China (863, 2015AA034601), the Fundamental Research Funds for the Central Universities, the Science and Technology Department of Hubei Province (No. 2017AAA190), the 111 Project (No. B07038), the Program for HUST Academic Frontier Youth Team (2016QYTD06), China Postdoctoral Science Foundation (2017M612452), and the Double first-class research funding of China-EU Institute for Clean and Renewable Energy (No. ICARE-RP-2018- SOLAR-001 and ICARE-RP-2018-SOLAR-002). M.A.R.P. is grateful to CONACyT/SENER Mexico for the financial support granted through the project 291195. The research leading to the results at the Delft University of Technology has received funding from the European Research Council Horizon 2020 ERC Grant Agreement no. 648433. We thank the Analytical and Testing Center of Huazhong University of Science and Technology (HUST) for various measurements. L.H. is grateful to Zaiwei Wang and Péter Péchy (EPFL), as well as Yue Hu and Yaoguang Rong (Wuhan National Lab), for helpful discussions and their support during the study.

The manuscript was written by L.H. and J.V.M. with the support of all authors. The project was conceptualized by M.G. with the support of J.V.M., who coordinated the project and led the investigation of the mode of action. L.H. performed the protonation of guanine, as well as thin film and device fabrication and characterization. P.A., M.M., F.J. and U.R. performed and analyzed the molecular dynamics simulations and DFT calculations, and D.J.K. and L.E. solid-state NMR measurements and analysis. M.C.G.-R. and F.G. performed the time-resolved microwave conductivity measurements and the analysis on samples prepared by M.A.R.-P. D.R. conducted the TEM measurements, A.U. the PL spectroscopy, L.P. the SEM measurements, C.T. single crystal XRD data, and Y.L. supported H.L. with synthesis. S.M.Z. and H.H. were involved in the discussion and provided support in project coordination, while M.G. directed the project.

Notes

The authors declare no competing interests. M.M. is also affiliated with the Scientific Computing Laboratory, Center for the Study of Complex Systems, Institute of Physics Belgrade, University of Belgrade, Pregrevica 118, 11080 Belgrade, Serbia.

Keywords: • hybrid perovskites • low-dimensional perovskites • guanine • solid-state NMR • perovskite solar cells

[1] M. Grätzel, *Nat. Mater.* **2014**, *13*, 838–842.
[2] Y. Rong, Y. Hu, A. Mei, H. Tan, M. I. Saidaminov, S. I. Seok, M. D. McGehee, E. H. Sargent, H. Han, *Science* **2018**, *361*, eaat8235–9.
[3] NREL Best Research Cell Efficiency Chart; https://www.nrel.gov/pv/assets/pdfs/best-research-cell-efficiencies.20190802.pdf (Accessed in August 2019).
[4] J. V. Milić, D. J. Kubicki, L. Emsley, M. Grätzel, *Chimia* **2019**, *73*, 317–323.
[5] N. Arora, M. I. Dar, M. Abdi-Jalebi, F. Giordano, N. Pellet, G. Jacopin, R. H. Friend, S. M. Zakeeruddin, M. Grätzel, *Nano Lett.* **2016**, *16*, 7155–7162.
[6] N. Pellet, P. Gao, G. Gregori, T.-Y. Yang, M. K. Nazeeruddin, J. Maier, M. Grätzel, *Angew. Chem. Int. Ed.* **2014**, *53*, 3151–3157.
[7] F. C. Hanusch, E. Wiesenmayer, E. Mankel, A. Binek, P. Angloher, C. Fraunhofer, N. Giesbrecht, J. M. Feckl, W. Jaegermann, D. Johrendt, et al., *J. Phys. Chem. Lett.* **2014**, *5*, 2791–2795.
[8] A. Amat, E. Mosconi, E. Ronca, C. Quarti, P. Umari, M. K. Nazeeruddin, M. Grätzel, F. De Angelis, *Nano Lett.* **2014**, *14*, 3608–3616.
[9] M. T. Weller, O. J. Weber, J. M. Frost, A. Walsh, *J. Phys. Chem. Lett.* **2015**, *6*, 3209–3212.
[10] A. Binek, F. C. Hanusch, P. Docampo, T. Bein, *J. Phys. Chem. Lett.* **2015**, *6*, 1249–1253.
[11] Z. Li, M. Yang, J.-S. Park, S.-H. Wei, J. J. Berry, K. Zhu, *Chem. Mater.* **2016**, *28*, 284–292.
[12] R. Hamaguchi, M. Yoshizawa-Fujita, T. Miyasaka, H. Kunugita, K. Ema, Y. Takeoka, M. Rikukawa, *Chem. Commun.* **2017**, *53*, 4366–4369.
[13] G. Li, T. Zhang, N. Guo, F. Xu, X. Qian, Y. Zhao, *Angew. Chem. Int. Ed.* **2016**, *128*, 13658–13662.
[14] J. Yan, W. Fu, X. Zhang, J. Chen, W. Yang, W. Qiu, G. Wu, F. Liu, P. Heremans, H. Chen, *Mater. Chem. Front.* **2018**, *2*, 121–128.
[15] J. V. Milić, J.-H. Im, D. J. Kubicki, A. Ummadisingu, J.-Y. Seo, Y. Li, M. A. Ruiz Preciado, M. I. Dar, S. M. Zakeeruddin, L. Emsley, M. Grätzel, *Adv. Energy Mater.* **2019**, *131*, 1900284.
[16] Y. Li, J. V. Milić, A. Ummadisingu, J.-Y. Seo, J.-H. Im, H.-S. Kim, Y. Liu, M. I. Dar, S. M. Zakeeruddin, P. Wang, M. Grätzel, *Nano Lett.* **2019**, *19*, 150–157.
[17] (a) G. Grancini, M. K. Nazeeruddin, *Nat. Rev. Mater.* **2018**, *4*, 4–22. (b) L. Mao, C. C. Stoumpos, M. G. Kanatzidis, *J. Am. Chem. Soc.* **2018**, *141*, 1171–1190.

[18] T. Carell, C. Behrens, J. Gierlich, *Org. Biomol. Chem.* **2003**, *1*, 2221–2228.
[19] T. Kawakami, T. Taniguchi, T. Hamamoto, Y. Kitagawa, M. Okumura, K. Yamaguchi, *Int. J. Quant. Chem.* **2005**, *105*, 655–671.
[20] J. C. Genereux, J. K. Barton, *Chem. Rev.* **2010**, *110*, 1642–1662.
[21] F. D. Lewis, R. M. Young, M. R. Wasielewski, *Acc. Chem. Res.* **2018**, *51*, 1746–1754.
[22] D. Prochowicz, M. Franckevičius, A. M. Cieślak, S. M. Zakeeruddin, M. Gratzel, J. Lewiński, *J. Mater. Chem. A* **2015**, *3*, 20772–20777.
[23] D. Prochowicz, P. Yadav, M. Saliba, M. Saski, S. M. Zakeeruddin, J. Lewiński, M. Gratzel, *Sust. Energy Fuels* **2017**, *1*, 689–693.
[24] D. J. Kubicki, D. Prochowicz, A. Hofstetter, P. Péchy, S. M. Zakeeruddin, M. Grätzel, L. Emsley, *J. Am. Chem. Soc.* **2017**, *139*, 10055–10061.
[25] D. J. Kubicki, D. Prochowicz, A. Hofstetter, S. M. Zakeeruddin, M. Grätzel, L. Emsley, *J. Am. Chem. Soc.* **2017**, *139*, 14173–14180.
[26] D. J. Kubicki, D. Prochowicz, A. Hofstetter, M. Saski, P. Yadav, D. Bi, N. Pellet, J. Lewiński, S. M. Zakeeruddin, M. Grätzel, L. Emsley, *J. Am. Chem. Soc.* **2018**, *140*, 3345–3351.
[27] D. J. Kubicki, D. Prochowicz, A. Hofstetter, S. M. Zakeeruddin, M. Grätzel, L. Emsley, *J. Am. Chem. Soc.* **2018**, *140*, 7232–7238.
[28] D. Bi, X. Li, J. V. Milić, D. J. Kubicki, N. Pellet, J. Luo, T. LaGrange, P. Mettraux, L. Emsley, S. M. Zakeeruddin, M. Grätzel, *Nat. Commun.* **2018**, *9*, 4482.
[29] M. M. Tavakoli, W. Tress, J. V. Milić, D. Kubicki, L. Emsley, M. Grätzel, *Energy Environ. Sci.* **2018**, *11*, 3310–3320.
[30] E. E. Bendeif, S. Dahaoui, N. Benali-Cherif, C. Lecomte, *Acta Cryst.* **2007**, *B63*, 448–458.
[31] K. N. Rogstad, Y. H. Jang, L. C. Sowers, W. A. Goddard, *Chem. Res. Toxicol.* **2003**, *16*, 1455–1462.
[32] H. Tsai, W. Nie, J.-C. Blancon, C. C. Stoumpos, R. Asadpour, B. Harutyunyan, A. J. Neukirch, R. Verduzco, J. J. Crochet, S. Tretiak, et al., *Nature* **2016**, *536*, 312–316.
[33] L. Mao, C. C. Stoumpos, M. G. Kanatzidis, *J. Am. Chem. Soc.* **2018**, *141*, 1171–1190.
[34] Y. Hu, M. F. Aygüler, M. L. Petrus, T. Bein, P. Docampo, *ACS Energy Lett.* **2017**, *2*, 2212–2218.
[35] E. Smecca, Y. Numata, I. Deretzis, G. Pellegrino, S. Boninelli, T. Miyasaka, A. La Magna, A. Alberti, *Phys. Chem. Chem. Phys.* **2016**, *18*, 13413–13422.
[36] W. S. Yang, J. H. Noh, N. J. Jeon, Y. C. Kim, S. Ryu, J. Seo, S. Il Seok, *Science* **2015**, *348*, 1230–1234.
[37] J. V. Passarelli, D. J. Fairfield, N. A. Sather, M. P. Hendricks, H. Sai, C. L. Stern, S. I. Stupp, *J. Am. Chem. Soc.* **2018**, *140*, 7313–7323.
[38] S. Maheshwari, T. J. Savenije, N. Renaud, F. C. Grozema, *J. Phys. Chem. C* **2018**, *122*, 17118–17122.
[39] M. C. Gélvez-Rueda, E. M. Hutter, D. H. Cao, N. Renaud, C. C. Stoumpos, J. T. Hupp, T. J. Savenije, M. G. Kanatzidis, F. C. Grozema, *J. Phys. Chem. C* **2017**, *121*, 26566–26574.
[40] R. Herckens, W. T. M. Van Gompel, W. Song, M. C. Gélvez-Rueda, A. Maufort, B. Ruttens, J. D'Haen, F. C. Grozema, T. Aernouts, L. Lutsen, D. Vanderzande, *J. Mater. Chem. A* **2018**, *6*, 22899–22908.

Entry for the Table of Contents

RESEARCH ARTICLE

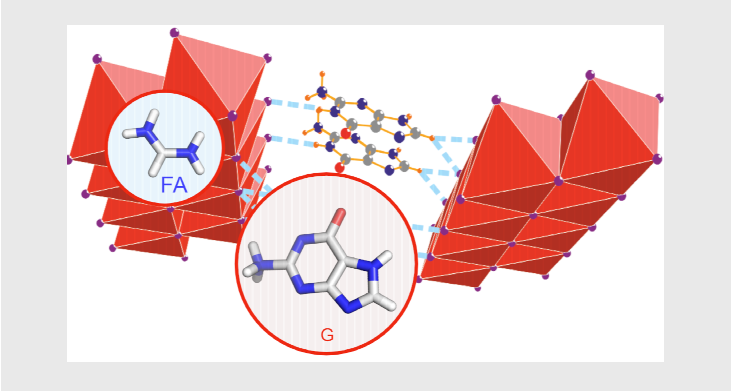

Guanine Perovskites: Stabilization of α-$FAPbI_3$ phase is realized by using guaninium (G) based G_2PbI_4 low-dimensional perovskites forming heterostructures that lead to improved performances and stabilities of the corresponding solar cells. The structural properties are investigated by means of solid-state NMR spectroscopy at the atomic level in conjunction with molecular dynamics simulations and DFT calculations, X-ray crystallography and high-resolution transmission electron microscopy to unravel the mode of action and set the path for using this approach in perovskite solar cell research.

*Li Hong, Jovana V. Milić, Paramvir Alhwat, Marko Maldenović, Dominik J. Kubicki, Farzaneh Jahanbakshi, Ran Den, María C. Gélvez-Rueda, Marco A. Ruiz-Preciado, Amita Ummadisingu, Yuhang Liu, Chengbo Tian, Linfeng Pan, Shaik M. Zakeeruddin, Anders Hagfeldt, Ferdinand C. Grozema, Ursula Roethlisberger, Lyndon Emsley, Hongwei Han*and Michael Graetzel**

Page 1 – Page 7

Guanine-Stabilized Formamidinium Lead Iodide Perovskites

[a] Li Hong, Prof. Hongwei Han
Wuhan National Lab for Optoelectronics
Wuhan, 430074 Hubei, China
E-mail: hongwei.han@mail.hust.edu.ch
[b] Li Hong, Dr. Jovana V. Milic*, Dr. Dominik J. Kubicki, Dr. Ran Dan, Dr. Amita Ummadisingu, Dr. Shaik M. Zakeeruddin, and Prof. Michael Graetzel*
Laboratory of Photonics and Interfaces
École Polytechnique Fédérale de Lausanne
Station 6, CH-1015 Lausanne, Switzerland
E-mail: jovana.milic@epfl.ch, michael.graetzel@epfl.ch
[c] Paramvir Ahlawat, Prof. Ursula Roethlisberger
Laboratory of Computational Chemistry and Biochemistry